Role of particle type and concentration on characteristics of PEO coatings on AM50 magnesium alloy

M. Mohedano[a], R. Arrabal[a], B. Mingo[b], A. Pardo[a], E. Matykina[a]*

[a] Departamento de Ciencia de Materiales, Facultad de Ciencias Químicas, Universidad Complutense, 28040, Madrid, Spain

[b] School of Materials, University of Manchester, Oxford Road, Manchester, M13 9PL, UK

**Corresponding author. Tel: 34 91 3945227; Fax: 34 91 3944357*

E–mail: mmohedan@ucm.es

Abstract

Composite ceramic coatings were formed on a magnesium alloy by AC plasma electrolytic oxidation using a phosphate-based electrolyte with α-Al_2O_3, monoclinic ZrO_2 or CeO_2 particles in suspension. Effects of particles concentration (2, 5 and 10 g/L) on the electrical response, composition/morphology and corrosion behaviour of the coatings were investigated. Findings revealed successful incorporation of particles, which were preferentially located in the outer coating layer. Due to high temperatures at the locations of microdischarges, zirconia particles underwent transformation from monoclinic to tetragonal structure. The majority of alumina and ceria particles remained unaffected, although some of the alumina particles possibly formed $MgAl_2O_4$ by reaction with the substrate. Porosity and thickness of the coatings tended to decrease with increasing particles concentration in the electrolyte. Coatings formed in the electrolytes containing CeO_2 particles revealed the best long-term corrosion performance in 0.5 wt. % NaCl solution.

Keywords

PEO; Particles; Magnesium; Characterization; Corrosion

1. Introduction

There are numerous studies on anodizing of magnesium alloys [1-3]. The main driving force behind such interest is to improve the corrosion resistance and, therefore, to exploit the excellent physical and mechanical properties of magnesium alloys, such as their high strength-to-mass ratio and damping capacity. In particular, plasma electrolytic oxidation (PEO) is receiving great attention as one of the most effective ways to coat Mg materials using an environmentally friendly process that confers the required improvement of corrosion and wear properties in one step [4,5]. The formation of PEO coatings involves polarization of the material to relatively high voltages with contributions from plasma-chemical, thermal and anodic oxidation processes [6]. Coating properties are mainly influenced by processing parameters (treatment time, electrical regime, electrical wave design) and the electrolyte composition [7,8].

Despite their excellent short-term corrosion resistance, PEO coatings on magnesium alloys are relatively porous and the inner barrier layer eventually fails after long-term corrosion testing [9]. Hence, most strategies acknowledged the need for optimization of PEO processes and electrolyte conditions and/or for application of post-treatments [10,11]. A novel approach to overcoming this problem consists in use of colloidal suspensions of ceramic particles so that they are incorporated into the coating at the locations of plasma microdischarges, reducing the coating porosity [12]. The mechanism of incorporation of particles into PEO coatings is still not clear, although it is generally agreed that particles migrate towards the anode due to electrophoretic and/or mechanical forces and then undergo reactive or inert incorporation depending on the nature of the particles and applied conditions [13].

Various kinds of particles (Al_2O_3, SiO_2, TiO_2, SiC, CeO_2, etc.) have been added into PEO coatings on magnesium alloys [12,14]. For instance, Al_2O_3 particles have shown to increase

the short-term corrosion resistance, wear resistance and scratch hardness due to formation of more compact coatings [15,16]. It also appears that these particles participate in chemical reactions during the PEO process resulting in formation of $MgAl_2O_4$ [15-17], although unaltered particles have also been observed [18].

Under DC and AC conditions, ZrO_2 particles are incorporated at the surface and followed by subsequent transport along short-circuit paths into the inner coating regions. Additionally, due to locally high temperatures, transition from monoclinic to tetragonal zirconia and formation of $Mg_2Zr_5O_{12}$ have also been observed, suggesting temperatures in the range of 1240 to 2100 ºC at the locations of microdischarges [19-22]. From a corrosion point of view, Lee [20], Gnedenkov [23] and Tang [22] reported improved corrosion resistance in PEO-coated magnesium alloys with incorporated ZrO_2 particles due to reduced coating porosity, whereas Mandelli [24] did not get satisfactory results, possibly due to negligible incorporation of particles into the coating.

The incorporation of CeO_2 particles into PEO coatings under DC regime has been explored by Lim [25] and Xiong [26]. Lim et al. observed an increased incorporation of CeO_2 particles at pores and cracks with the increasing CeO_2 concentration in the electrolyte from 10 to 30 g/L. They also found that 30 g/L CeO_2 in the electrolyte yielded the highest corrosion potential and lowest corrosion current density, possibly due to the reduced coating porosity and high chemical stability of CeO_2. This is similar to the results by Xiong et al. who also observed inert incorporation of CeO_2 particles during the PEO process. A partial reactive incorporation of CeO_2 particles under AC electrical conditions was reported in author´s previous work [27], which points out that not only the electrolyte composition but also the electrical parameters play an important role in the final morphology and composition of the coating. That work revealed that low concentration of CeO_2 in the electrolyte (3 g/L) partially blocked the pores

in the coating leading to improved corrosion properties. Higher concentration of CeO_2 in the electrolyte (10 g/L) changed the characteristics of local microdischarges generating coatings with more heterogeneous microstructure and a higher number of unsealed pores and cracks.

Most of the previous studies of PEO containing particles do not take into consideration the effect of particles concentration on the electrical response and/or long-term corrosion performance of the coatings. In addition, it is not common to compare different particles for an individual electrolyte, and in particular, for electrolytes with fluoride species, as most of the work has been done in fluoride-free electrolytes [12,13,22,27]. Therefore, in the present study, the effects of α-Al_2O_3, ZrO_2 and CeO_2 particles (2, 5 and 10 g/L) in fluoride-containing phosphate electrolyte on the electrical response, morphology, composition and corrosion behaviour of PEO coatings on AM50 magnesium alloy have been investigated.

2. Material and methods

2.1. Materials

AM50 magnesium alloy (4.5% Al, <0.26% Mn, <0.2% Zn, <0.004% Fe and balance Mg in weight percent), of size 30 mm × 25 mm × 3 mm supplied by Magnesium Elektron Ltd., was used as substrate for PEO. Specimens were ground to P1200 grit silicon carbide and a working area of ~2 cm^2 was defined by application of Lacquer 45 resin (MacDermid plc).

2.2. PEO treatment

PEO treatment was carried out for 900 s using an EAC-S2000 power supply (ET Systems electronic) with a square electrical signal (50 Hz, +420 V/-60 V, 50% duty cycle), an initial ramp of 60 s and a root mean square (rms) current density limit of 250 mA/cm^2. The electrolyte, comprising 10 g/L $Na_3PO_4 \cdot 12H_2O$, 1 g/L KOH and 8 g/L NaF, prepared from deionised water and high-purity chemicals, was continuously stirred during the treatment. Additions of 2, 5 and 10 g/L of α-Al_2O_3 (~300 nm, Buehler), ZrO_2 (300-700 nm, Inframat

Advanced Materials) or CeO_2 (~560 nm, Inframat Advanced Materials) were made as required. The coatings were formed in a 2 L double-walled glass cell through which cooled water was pumped in order to maintain the electrolyte temperature close to 20 ºC. A sheet of type 316 stainless steel, with the dimensions of 7.5 × 15 cm, was used as the counter-electrode. After PEO treatment, the specimens were rinsed in deionised water and dried in warm air.

2.3 Characterization

Surface and cross-sectional morphologies of PEO coatings were examined by scanning electron microscopy using a JEOL JSM-6400 instrument equipped with Oxford Link energy-dispersive X-ray (EDS) microanalysis hardware. Phase composition was investigated by X-ray diffraction (XRD) using a Philips X´Pert-MPD (PW 3040) instrument with a Bragg-Brentano geometry and a step size of 0.005º in the 2θ range from 10° to 80°. Provided XRD patterns of PEO coatings with incorporated particles correspond to those formed in the electrolytes with 5 g/L of particles.

The thicknesses of the coatings were measured at 20 randomly selected places using an eddy-current meter (Isoscope FMP10, Fischer). Surface roughness was measured over a distance of 15 mm in five different locations using a Surtronic 25 tester (Taylor Hobson Precision) and TalyProfile software applying a Gaussian filter of 2.5 mm.

2.4 Electrochemical tests

A Gill AC computer-controlled potentiostat (ACM Instruments) equipped with a frequency response analyzer and connected to a three-electrode cell was used for the electrochemical measurements. The working electrode was the test material with an immersed area of 1 cm^2. Graphite and silver/silver chloride (Ag/AgCl, 3M KCl) electrodes were used as the counter

and reference electrodes, respectively. The test solution consisted of naturally-aerated 0.5 wt.% NaCl solution at room temperature (22 ºC). EIS measurements were conducted at various times up to 7 days of immersion. The frequency range was from 30 kHz to 10 mHz and the amplitude of the sinusoidal potential signal was 10 mV with respect to the open circuit potential (OCP). Measurements were performed at least twice to ensure reproducibility of the results.

3. Results and discussion

3.1. Coating Characterization

Figure 1 depicts the typical *rms* current-time transients during the different PEO treatments. Without particles in the electrolyte, PEO coating reveals a current drop after 450 s of processing (Fig.1 a), which is a common feature under voltage-controlled mode. This drop is related to an increase of the coating impedance and consequently the higher resistance of the oxide material to mass transfer [28].

The addition of ZrO_2 particles into the bath shifts the current drop to earlier times, *e.g.* for 2 g/L the drop occurs after 330 s and is further reduced to 190 s for 10 g/L (Fig.1 b). A more significant effect is observed in the case of Al_2O_3 particles, with current drop times of 280 s and 120 s for concentrations of 2 g/L and 10 g/L respectively. The incorporation of 2 g/L CeO_2 reveals only a slight difference in the current drop compared to the electrolyte without particles, but this difference increases for higher concentrations of CeO_2 with a current drop time of 280 s for PEO-10g/L CeO_2.

It ought to be mentioned that most of the studies reported in the literature do not disclose the influence of particles on the electrical response of the PEO process, focusing instead on the mechanisms of incorporation and/or the final coating properties such as corrosion, wear and photovoltaic behaviour [12]. When electrical parameters (current/votage) and the coating growth rate are disclosed, the results are usually controversial [17,25,29-31]. This is associated with the wide range of different processing parameters (voltage, current, pulse

form, frequency and duty cycle) that can be used which directly influence the individual and collective characteristics of the micro discharges, affecting the resultant coating [32]. The systematic study performed in the present work reveals that, under AC voltage control, there is an early current drop for all PEO treatments with suspended particles and furthermore it is influenced by both the nature and concentration of the particles.

Scanning electron micrographs of the coating formed in the particle-free electrolyte are shown in Figure 2 with the corresponding EDS point analysis along the thickness of the coating gathered in Table 1. The plan view (Fig. 2 a) reveals the typical PEO features, *i.e.* volcano-like pores and microcracks formed after rapid solidification of molten material in the discharge channels [33]. In the cross-section (Fig. 2b), the coating reveals a three-layered structure with an outer part (less than 50% of the coating thickness) appearing to be more compact but with bigger pores than the inner fluoride-rich layer (Table 1). The latter is typical of PEO coatings formed in phosphate/fluoride-based electrolytes [34]. Next to the substrate appears a micrometre-thick barrier layer (detail in Fig. 2c) mainly composed of Mg, O and F (Table 1); such thickness and uniformity of the barrier layer, important for corrosion performance, is uncommon for PEO coatings on Mg obtained in any but fluoride-based electrolytes [35-37].

Figures 3, 4 and 5 show the plan views and cross-sections of the coatings formed in the electrolytes with suspended particles. The location of ZrO_2 and CeO_2 particles is clearly distinguishable as brighter regions, whereas Al_2O_3 particles are not readily visible. This is mainly related to two factors: *(i)* the atomic number contrast and *(ii)* the incorporation mechanism of the particles that, in case of Al_2O_3, is reactive. The EDS analyses of the coatings in the outer and inner parts are shown in Table 1 and thickness, roughness and pore area are gathered in Table 2.

The addition of ceramic particles into the electrolyte results in some common features for all the PEO coatings that can be summarized as follows:

i) The size and population density of the surface pores decreased with increasing particles concentration (from 2 g/L to 10 g/L), leading to smoother coatings. The change in morphology can be clearly observed in the SEM plan views (Fig 2 a and Fig. 3-5 a,c,e); it is more significant for addition of ZrO_2 and Al_2O_3 particles, with the highest decrease in the pore area (from 7 to 1.5% for ZrO_2). This sealing effect has been already observed for other particles such as Si_3N_4 or clay [38,13] and it is associated with the individual characteristics of the microdischarges and the preferential location of particles in the pores of the coatings [19,39].

ii) Electrolytes containing particles lead to the formation of thinner coatings, as can be observed in the SEM cross-sections (Fig. 3-5 b,d,f). Thickness decreases by about ~25, ~35 and ~36 μm for ZrO_2, Al_2O_3 and CeO_2 particles when their concentration increases from 2 to 10 g/L in the electrolyte. These results are in concordance with the earlier current drop (Fig. 1) and is a direct consequence of the change in the nature of the microdischarges due to the presence of particles in the electrolyte. The analysis of cross-sections (Fig. 3-5 b,d,f) also reveals that increasing the amount of particles in the electrolyte improves the quality of the barrier layer.

iii) Particles are preferentially incorporated in the outer coating regions, with increasing amounts of Zr, Al and Ce species for higher concentration of particles in the electrolyte (Table 2). The reduced number of particles in the inner region indicates a limited inward mass transfer. This feature was also observed in a

similar study using fluoride-free electrolyte with ZrO_2 and is typical of AC PEO coatings. This has been associated with the small diameter of the discharge channel during "soft" sparking [40].

XRD studies for different PEO coatings (without and with particle additions) are shown in Figure 6. XRD patterns of PEO coatings with incorporated particles correspond to those formed in the electrolytes with a particle concentration of 5 g/L (Electrolytes with 2 and 10 g/L gave similar results and are not included here). The studies reveal the presence of MgO and MgF_2 as well as inertly incorporated ZrO_2, α-Al_2O_3 and CeO_2 particles, which is expected considering their high melting points (2700 ºC, 2072 ºC and 2600 ºC, respectively). In the case of ZrO_2 and Al_2O_3 there is also some reactive incorporation as indicated by the presence of tetragonal ZrO_2 and $MgAl_2O_4$, the latter evidently in a very small amount as indicated by its low intensity peaks. Monoclinic zirconia transforms to tetragonal zirconia at a temperature of 1239 ºC, whereas $MgAl_2O_4$ normally requires solid-state reaction between MgO and Al_2O_3 at temperatures above 1400 ºC [41]. Contrary to previous studies [40], neither cubic zirconia nor $Mg_2Zr_5O_{12}$ were detected by XRD. This suggests lower temperatures in the discharges in the present study, as cubic zirconia normally forms above 2370 ºC and $Mg_2Zr_5O_{12}$ at temperatures above 1850 ºC. In the MgO-CeO_2 system, ternary phases are not reported but there is a eutectic reaction at 2100 ºC which could result in some reactive incorporation of CeO_2 particles [27]. However, the lack of a eutectic MgO-CeO_2 aggregate and the discrete morphology of CeO_2 particles suggests temperatures below 2100 ºC. Therefore, under the studied conditions, it is presumed here that the temperature of the coating material in the discharge channels rose to at least ~1400 ºC.

3.2. Electrochemical behavior

To evaluate the degradation behavior of all studied materials (PEO coatings with and without incorporated particles and the substrate) the evolution of the impedance modulus (at 0.1 Hz) with the immersion time in 0.5 wt.% NaCl solution has been monitored (Figure 7).

At early stages of immersion, PEO coating formed in the particle-free electrolyte reveals higher corrosion resistance compared to the bare material, with values of the modulus of the impedance of 10^4 Ω cm^2 (Fig. 7 a). However, a considerable decrease of the impedance modulus is observed after 7 days of immersion, reaching values similar to those of the substrate due to coating failure (manifested as surface pitting). This reduction of protective properties is associated with the penetration of the electrolyte through cracks and pores of the oxide layer leading to chemical degradation.

PEO coatings developed in electrolytes containing particles reveal superior anticorrosion properties for all immersion times in comparison with both PEO particle-free coating and the bare material, which can be partly explained by their lower porosity.

At the beginning of the immersion (after 1h), PEO coatings with added Al_2O_3 (Fig. 7 c) show the best performance with the highest value of the impedance modulus (2.5×10^6 Ω cm^2) for particles concentration of 10 g/L. This better short-term behaviour is related to the lower pore area (Table 2) that strongly influences the initial steps of corrosion process delaying the penetration of the electrolyte. PEO coatings containing ZrO_2 and CeO_2 particles (Fig. 7 b,d) reveal similar values of the modulus of the impedance, in the range of 2×10^5 Ω cm^2 to 4×10^5 Ω cm^2, without a clear effect of the particles concentration on the short-term (<24 h) corrosion performance.

For longer immersion times (up to 7 days), a different response on the corrosion behaviour is observed for the oxide layers depending on the nature of particles and their concentration. In the case of PEO layers with ZrO_2 particles, a gradual degradation occurs without any significant effect of the amount of particles incorporated into the coating. These coatings show better corrosion performance (with higher values of the impedance modulus) than the particle-free coating but a similar trend with the immersion time, also indicating a gradual corrosion process. Lee et al. [20] also reported an improvement of the corrosion properties of PEO coating with ZrO_2 nanoparticles (9 g/L ZrO_2) due to the lower porosity of the coating, but the effect of particles concentration was not evaluated. The present study points out that increasing the concentration of ZrO_2 particles from 2 to 10 g/L does not yield a great improvement in the corrosion performance.

The addition of Al_2O_3 particles also improves the corrosion behaviour of PEO coatings compared with the PEO particle-free oxide layer. This beneficial effect was already reported by Zhang et al. [18] and Wang et al. [16] following the incorporation of Al_2O_3 particles into PEO coatings on AZ91 and AZ31 Mg alloys, respectively. However, in the first work, the influence of particles concentration was not evaluated and in both studies the long-term performance remained unclear. Findings of the present investigation reveal an improvement in the short-term corrosion properties of PEO coatings formed in electrolytes with Al_2O_3 concentrations higher than 5 g/L, which is in concordance with the work conducted by Wang et al. [16] and it is associated with the lower porosity of the outer oxide layer, delaying the electrolyte penetration. The better long-time behaviour of the coatings with higher amount of Al_2O_3 particles is related to the increase of Al in the oxide layer (Table 1) and the formation of more thermodynamically stable phases decreasing the chemical degradation of the oxide layer.

PEO coatings containing CeO_2 particles reveal the best long-term corrosion performance, characterized by a stabilization of the obtained results with the exposure time. This tendency indicates a long-term protection effect and better corrosion properties compared with other oxide layers containing particles. This fact could be associated with an active protective character of PEO coatings containing Ce species: during the degradation process of the coating some of the Ce containing products may convert into Ce^{3+} ions that have been claimed to have a "self-healing" effect [11,27].

4. Conclusions

Composite ceramic-like coatings were developed on AM50 Mg alloy using a phosphate-based electrolyte with α-Al_2O_3, monoclinic ZrO_2 or CeO_2 particles in suspension. PEO treatments with suspended particles show an early drop of the current during PEO related to a faster increase of the impedance of the oxide layer.

ZrO_2, α-Al_2O_3 and CeO_2 particles are preferentially incorporated into the outer layer of the coatings. With the increase of the amount of particles, from 2 g/L to 10 g/L, the thickness and roughness of the coatings as well as the size and the population density of the surface pores decreased. Temperatures of the order of ~1400ºC at the location of microdischarges promote the formation of tetragonal zirconia and $MgAl_2O_4$ in the coatings with incorporated ZrO_2 and Al_2O_3 particles, respectively.

PEO coatings developed in particles containing electrolytes reveal superior anticorrosion properties for all immersion times in comparison to both PEO particle-free layers and the bare material. The addition of CeO_2 particles into the electrolyte leads to the formation of PEO coatings with improved long-term corrosion performance compared with coatings containing other particles (Al_2O_3 and ZrO_2) which could be associated with a self-healing mechanism.

For this type of PEO coatings, particles concentration below 10 g/L is sufficient in order to improve the corrosion behaviour of magnesium alloys.

Acknowledgments

MM is grateful to the MINECO (Spain) for financial support via Proyecto Retos Jovenes Investigadores (MAT2015-73355-JIN). This work has been financial supported by Comunidad de Madrid (MULTIMAT-CHALLENGE, Ref: P2013/MIT-2862) and MINECO/FEDER (Spain, Project MAT2015-66334-C3-3-R).

References

1. Y. Liu, F. Yang, Z. Wei, Z. Zhang. Anodizing of AZ91D magnesium alloy using environmental friendly alkaline borate-biphthalate electrolyte, Trans. Nonferrous Met. Soc. China, 22 (2012) 1778-1785.

2. X.H. Guo, M.Z. An, P.X. Yang, H.X. Li, C.N. Su, Effects of benzotriazole on anodized film formed on AZ31B magnesium alloy in environmental-friendly electrolyte, J. Alloys Compd., 482 (1–2) (2009) 487-497.

3. A. Němcová, O. Galal, P. Skeldon, I. Kuběna, M. Šmíd, E. Briand, I. Vickridge, J-J. Ganem, H. Habazaki, Film growth and alloy enrichment during anodizing AZ31 magnesium alloy in fluoride/glycerol electrolytes of a range of water contents, Electrochim. Acta, 219 (2016) 28-37.

4. K. M. Lee, Y. S. Kim, H. W. Yang, J. H. Park, Y. G. Ko, D. H. Shin, Formation of ZrO_2 in coating on Mg–3 wt.%Al–1 wt.%Zn alloy via plasma electrolytic oxidation: Phase and structure of zirconia, Mater. Charact., 99 (2015) 101-108.

5. L.R. Krishna, G. Poshal, A. Jyothirmayi, G. Sundararajan, Relative hardness and corrosion behavior of micro arcoxidation coatings deposited on binary and ternary magnesium alloys, Mater. Des., 77 (2015) 6-14.

6. V.I. Belevantsev, O.P. Terleeva, G.A. Markov, E.K. Shulepko, A.I. Slonova, V.V. Utkin, Micro-plasma electrochemical processes, Prot. Met., 34 (1998) 416-430.

7. M. Tarakci, Plasma electrolytic oxidation coating of synthetic Al–Mg binary alloys, Mater. Charact., 62 (2011) 1214-1221.

8. A.L. Yerokhin, X. Nie, A. Leyland, A. Matthew, Characterisation of oxide films produced by plasma electrolytic oxidation of a Ti-6Al-4V alloy, Surf. Coat. Technol., 130 (2000) 195-206.

9. R. Arrabal, E. Matykina, F. Viejo, P. Skeldon, G.E. Thompson, Corrosion resistance of WE43 and AZ91D magnesium alloys with phosphate PEO coatings, Corros. Sci. 50 (2008) 1744-1752.

10. D.K. Ivanou, M. Starykevich, A.D. Lisenkov, M.L. Zheludkevich, H.B. Xue, S.V. Lamaka, M.G.S. Ferreira, Plasma anodized ZE41 magnesium alloy sealed with hybrid epoxy-silane coating, Corr. Sci. 730(2013) 300-308.

11. M. Mohedano, C. Blawert, M.L. Zheludkevich, Cerium-based sealing of PEO coated AM50 magnesium alloy, Surf. Coat. Tech., 269 (2015) 145-154.

12. X. Lu, M. Mohedano, C. Blawert, E. Matykina, R. Arrabal, K. U.Kainer, M.L. Zheludkevich, Plasma electrolytic oxidation coatings with particle additions – A review, Surf. Coat. Tech., 307 (2016) 1165-1182.

13. X. Lu, S.P. Sah, N. Scharnagi, M. Störmer, M. Starykevich, M. Mohedano, C. Blawert, M.L. Zheludkevich, K.U. Kainer, Degradation behavior of PEO coating on AM50 magnesium alloy produced from electrolytes with clay particle addition, Surf. Coat. Tech., 269 (2015) 155-169.

14. D.V. Mashtalyar, S.V. Gnedenkov, S.L. Sinebryukhov, I.M. Imshinetskiy, A.V. Puz, Plasma electrolytic oxidation of the magnesium alloy MA8 in electrolytes containing TiN nanoparticles, J. Mater. Sci. Technol., http://dx.doi.org/10.1016/j.jmst.2017.01.021

15. M. Laleh, A.S. Rouhaghdam, T. Shahrabi, A. Shanghi, Effect of alumina sol addition to micro-arc oxidation electrolyte on the properties of MAO coatings formed on magnesium alloy AZ91D, J. Alloy Compd., 496 (2010) 548-552.

16. Y. Wang, D. Wei, J. Yu, S. Di, Effects of Al_2O_3 Nano-additive on Performance of Micro-arc Oxidation Coatings Formed on AZ91D Mg Alloy, J. Mater. Sci. Technol., 30 (2014) 984-99.

17. X. Li, B.L. Luan, Discovery of Al_2O_3 particles incorporation mechanism in plasma electrolytic oxidation of AM60B magnesium alloy, Mater. Lett. 86 (2012) 88-91.

18. D. Zhang, Y. Gou, Y. Liu, X. Guo, A composite anodizing coating containing superfine Al_2O_3 particles on AZ31 magnesium alloy, Surf. Coat. Tech., 236 (2013) 52-57.

19. R. Arrabal, E. Matykina, F. Viejo, P. Skeldon, G.E. Thompson, M.C. Merino, AC plasma electrolytic oxidation of magnesium with zirconia nanoparticles, Appl. Surf. Sci. 254 (2008) 6937-6942.

20. K.M. Lee, K.R. Shin, S. Namgung, B. Yoo, D.H. Shin, Electrochemical response of ZrO_2-incorporated oxide layer on AZ91 Mg alloy processed by plasma electrolytic oxidation, Surf. Coat. Tech., 205 (2011) 3779-3784.

21. K.M. Lee, B. U. Lee, S.I. Yoon, E.S. Lee, B. Yoo, D.H. Shin, Evaluation of plasma temperature during plasma oxidation processing of AZ91 Mg alloy through analysis of the melting behavior of incorporated particles, Electrochim. Acta 67 (2012) 6-11.

22. M. Tang, H. Liu, W. Li, L. Zhu, Effect of zirconia sol in electrolyte on the characteristics of microarc oxidation coating on AZ91D magnesium, Mater. Lett. 65 (2011) 413-415.

23. S.V. Gnedenkov, S.L. Sinebryukhov, D.V. Mashtalyar, I.M. Imshinetskiy, A.S. Gnedenkov, A.V. Samokhin, Y.V. Tsvetkov, Protective composite coatings obtained by plasma electrolytic oxidation on magnesium alloy MA8, Vacuum 120 (2015) 107-114.

24. A. Mandelli, M. Bestetti, A. Da Forno, N. Lecis, S.P. Trasatti, M. Trueba, Protective composite coatings obtained by plasma electrolytic oxidation on magnesium alloy MA8, Surf. Coat. Tech., 205 (2011) 4459-4465.

25. T.S. Lim, H.S. Ryu, S-H. Hong, Electrochemical corrosion properties of CeO2-containing coatings on AZ31 magnesium alloys prepared by plasma electrolytic oxidation, Corr. Sci., 62 (2012) 104-111.

26. Y. Xiong, C. Lu, C. Wang, R. Song, The n-MAO/EPD bio-ceramic composite coating fabricated on ZK60 magnesium alloy using combined micro-arc oxidation with electrophoretic deposition, Appl. Surf. Sci. 322 (2014) 230-235.

27. M. Mohedano, C. Blawert, M.L. Zheludkevich, Silicate-based Plasma Electrolytic Oxidation (PEO) coatings with incorporated CeO_2 particles on AM50 magnesium alloy, Mater. Des. 86 (2015) 735-744.

28. E. Matykina, R. Arrabal, A. Pardo, M. Mohedano, B. Mingo, I. Rodríguez, J. González, Energy-efficient PEO process of aluminium alloys, Mater. Lett. 127 (2014) 13-16.

29. K.M. Lee, Y.G. Ko, D.H. Shin, Incorporation of multi-walled carbon nanotubes into the oxide layer on a 7075 Al alloy coated by plasma electrolytic oxidation: coating structure and corrosion properties, Curr. Appl. Phys., 11 (2011) 55-59.

30. W. Li, M. Tang, L. Zhu, H. Liu, Formation of microarc oxidation coatings on magnesium alloy with photocatalytic performance, Appl. Surf. Sci. 258 (2012) 10017-10021.

31. X. Lu, C. Blawert, Y. Huang, H. Ovri, M.L. Zheludkevich, K.U. Kainer, Plasma electrolytic oxidation coatings on Mg alloy with addition of SiO_2 particles, Electrochim. Acta, 187 (2016) 20-33.

32. V. Dehnavi, B.L. Luan, X.Y. Liu, D.W. Shoesmith, S. Rohani, Correlation between plasma electrolytic oxidation treatment stages and coating microstructure on aluminium under unipolar pulsed DC mode, Surf. Coat. Technol., 269 (2015) 91-99.

33. L. Yerokhin, X. Nie, A. Leyland, A. Matthews, A.S.J. Dowey, Plasma electrolysis for surface engineering, Surf. Surf. Coat. Technol., 122 (1999) 73-93.

34. H. Habazaki, K. Fushimi, K. Shimizu, P. Skeldon, G. E. Thompson, Fast migration of fluoride ions in growing anodic titanium oxide, Electrochem. Commun., 9 (2007) 1222-1227.

35. B. Kazanski, A. Kossenko, M. Zinigrad, A. Lugovskoy, Fluoride ions as modifiers of the oxide layer produced by plasma electrolytic oxidation on AZ91D magnesium alloy, Appl. Surf. Sci., 287 (2013) 461-466.

36. F. Liu, J. Yu, Y. Song, D. Shan, E.H. Han, Effect of potassium fluoride on the in-situ sealing pores of plasma electrolytic oxidation film on AM50 Mg alloy, Mater. Chem. Phys., 162 (2015) 452-460.

37. M. Mohedano, B.J.C. Luthringer, B. Mingo, F. Feyerabend, R. Arrabal, P.J.Sanchez-Egido, C. Blawert, R. Willumeit-Römer, M.L. Zheludkevich, E. Matykina, Bioactive plasma electrolytic oxidation coatings on Mg-Ca alloy to control degradation behaviour, Surf. Coat. Tech., 315 (2017) 454-467.

38. X. Lu, C. Blawert, N. Scharnagl, K.U Kainer, Influence of incorporating Si_3N_4 particles into the oxide layer produced by plasma electrolytic oxidationon AM50 Mg alloy on coating morphology and corrosion properties, J. Magnes. Alloys, 1 (2013) 267-274.

39. C.S. Dunleavy, I.O. Golosnoy, J.A. Curran, T.W. Clyne, Characterisation of discharge events during plasma electrolytic oxidation, Surf. Surf. Coat. Technol., 203 (2009) 3410-3419.

40. E. Matykina, R. Arrabal, P. Skeldon, G.E. Thompson, Investigation of the growth processes of coatings formed by AC plasma electrolytic oxidation of aluminium, Electrochim. Acta 54 (2009) 6767-6778.

41. K. Yanagida, Y. Yamaguchi, K. Fujimoto, S. Ito, Low-Temperature Synthesis of $MgAl_2O_4$ by Capsule HIP Using Hydroxides as Starting Materials, Key Eng. Mater., 617 (2014) 217-220.

Tables

Table1. EDS analysis (at.%) of the coatings formed on magnesium alloy AM50 with and without incorporated ZrO_2, Al_2O_3 and CeO_2 particles.

Coating	Particles (g/L)	Location	Elements (at.%)							
			Mg	Al	O	F	Na	P	K	Zr or Ce
PEO	0	Surface	22.63	0.48	36.21	24.84	22.63	5.26	0.23	
		Inner	25.00	1.14	29.03	28.97	7.88	6.55	0.31	
		Barrier	46.56	1.85	15.48	33.90	-	1.45	-	
ZrO_2	2	Surface	17.61	0.69	39.36	25.11	8.85	4.32	0.22	3.36
		Inner	30.25	1.30	20.38	39.64	5.94	1.18	0.08	1.24
	5	Surface	14.25	0.28	47.56	20.38	8.44	-	0.22	8.81
		Inner	33.96	1.92	29.43	23.83	1.77	5.77	-	1.33
	10	Surface	24.85	0.32	38.16	18.79	7.43	-	0.21	9.84
		Inner	33.89	5.60	30.48	22.70	2.03	3.85	0.17	1.27
		Barrier	48.14	4.54	22.84	20.61	0.18	2.33	-	0.15
Al_2O_3	2	Surface	15.96	7.96	40.49	21.54	8.72	4.14	0.23	
		Inner	27.17	4.20	26.38	30.84	4.16	4.96	0.20	
	5	Surface	11.94	15.44	51.64	11.97	5.20	2.89	0.21	
		Inner	28.44	8.24	28.03	27.19	1.35	4.16	-	
	10	Surface	8.72	20.74	57.44	7.19	3.35	2.09	0.12	
		Inner	31.16	5.01	22.96	33.58	-	4.73	-	
		Barrier	43.55	3.46	20.94	29.60	-	2.44	-	
CeO_2	2	Surface	20.37	0.73	34.25	27.00	10.09	4.64	0.24	2.03
		Inner	31.80	2.23	22.32	34.40	3.18	5.40	0.10	0.57
	5	Surface	21.88	0.53	38.61	20.46	8.37	4.50	0.21	4.33
		Inner	30.38	1.59	27.33	31.37	2.19	4.78	-	0.62
	10	Surface	17.56	-	45.22	14.42	8.28	3.98	0.27	9.06
		Inner	30.13	0.91	27.41	31.13	2.55	4.82	-	1.28
		Barrier	52.73	0.97	15.30	31.00	-	-	-	-

Table 2. The main characteristics of the PEO coatings: thickness, roughness and porosity.

Coating	Particles (g/L)	Thickness (µm)	Ra (µm)	Rz (µm)	% area with pores
PEO	0	112 ± 12	6.7 ± 0.2	38 ± 1	7
ZrO_2	2	81 ± 5	5.9 ± 0.8	36 ± 5	3
	5	57 ± 4	5.1 ± 0.3	31 ± 2	1.5
	10	55 ± 4	5.3 ± 0.5	31 ± 4	<1.5
Al_2O_3	2	62 ± 5	5.2 ± 0.8	30 ± 3	5
	5	31 ± 3	3.4 ± 0.3	22 ± 2	1.5
	10	27 ± 3	3.3 ± 0.1	21 ± 1	<1.5
CeO_2	2	90 ± 7	6.6 ± 0.9	37 ± 5	7
	5	73 ± 5	5.2 ± 0.3	30 ± 1	7
	10	54 ± 3	4.3 ± 0.1	28 ± 2	3

Figure caption

Figure 1. *Rms* current-time transients during the different PEO treatments: (a) PEO without particles, (b) PEO+ZrO_2, (c) PEO+α-Al_2O_3, (d) PEO+ CeO_2.

Figure 2. Secondary electron images of the PEO coating without particles: (a) plan view (b) cross section, (c) detail of barrier layer.

Figure 3. Secondary electron images of the PEO coatings with ZrO_2 particles added in the electrolyte: (a,b) plan view and cross section of PEO+ 2g/L ZrO_2 , (c,d) plan view and cross section of PEO+ 5g/L ZrO_2, (e,f) plan view and cross section of PEO+ 10g/L ZrO_2.

Figure 4. Secondary electron images of the PEO coatings with α-Al_2O_3 particles added in the electrolyte: (a,b) plan view and cross section of PEO+ 2g/L α-Al_2O_3 , (c,d) plan view and cross section of PEO+ 5g/L α-Al_2O_3, (e,f) plan view and cross section of PEO+ 10g/L α-Al_2O_3.

Figure 5. Secondary electron images of the PEO coatings with CeO_2 particles added in the electrolyte: (a,b) plan view and cross section of PEO+ 2g/L CeO_2, (c,d) plan view and cross section of PEO+ 5g/L CeO_2, (e,f) plan view and cross section of PEO+ 10g/L CeO_2.

Figure 6. XRD patterns for PEO coatings without and with 5 g/L of particles addition.

Figure 7. Evolution of the impedance modulus (at 0.1 Hz) with the immersion time in 0.5 wt.% NaCl (a) PEO without particles, (b) PEO+ZrO_2, (c) PEO+α-Al_2O_3, (d) PEO+ CeO_2.

Figures

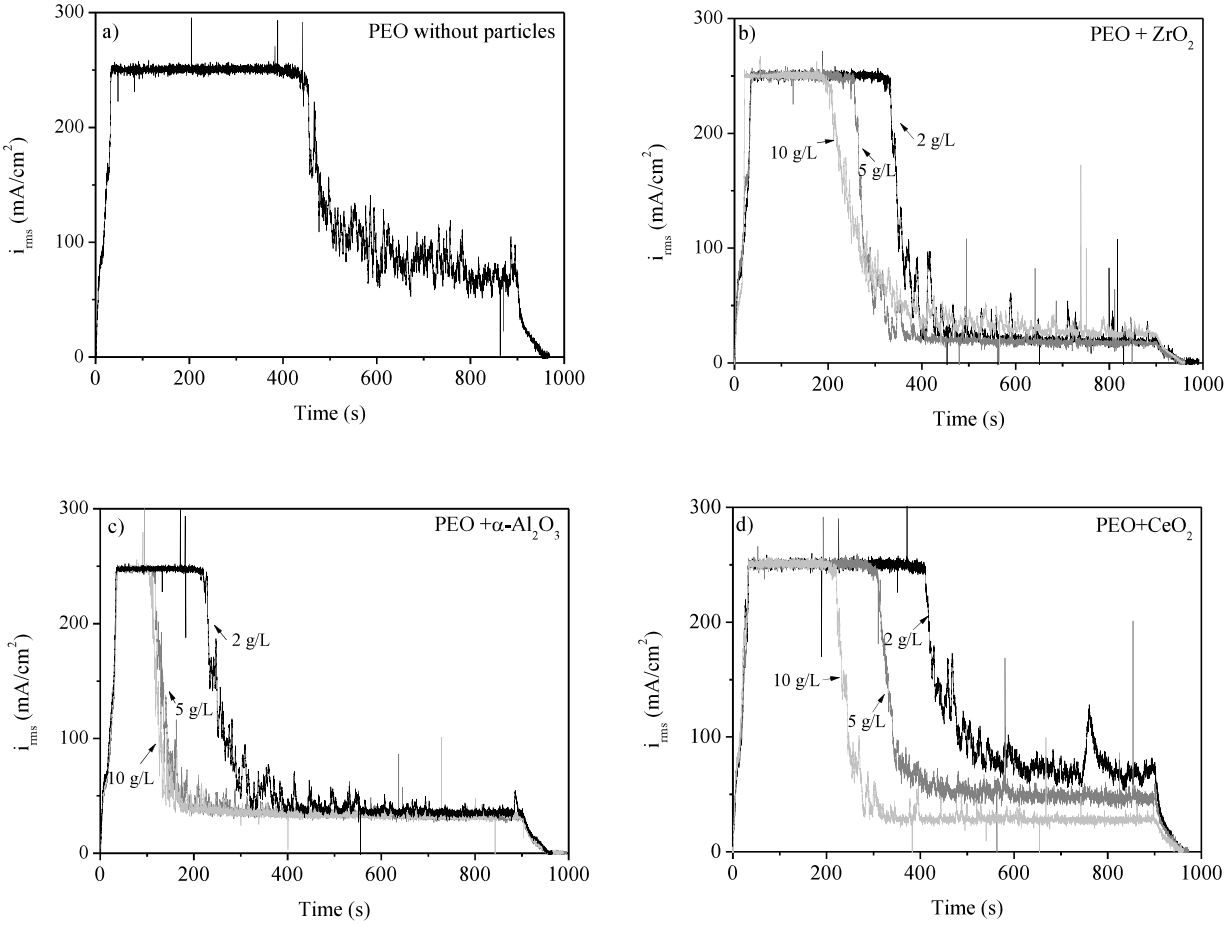

Figure 1.

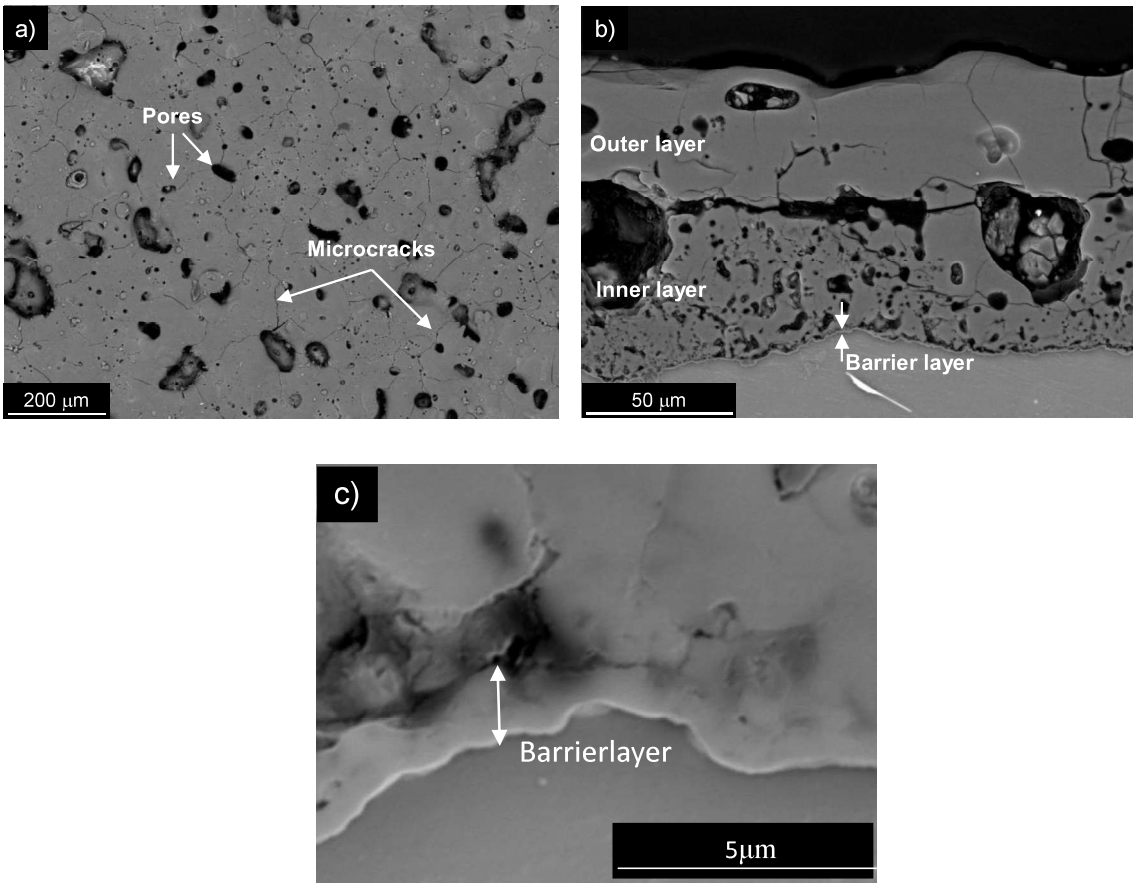
a)
Pores
Microcracks
200 µm
b)
Outer layer
Inner layer
Barrier layer
50 µm
c)
Barrierlayer
5µm

Figure 2.

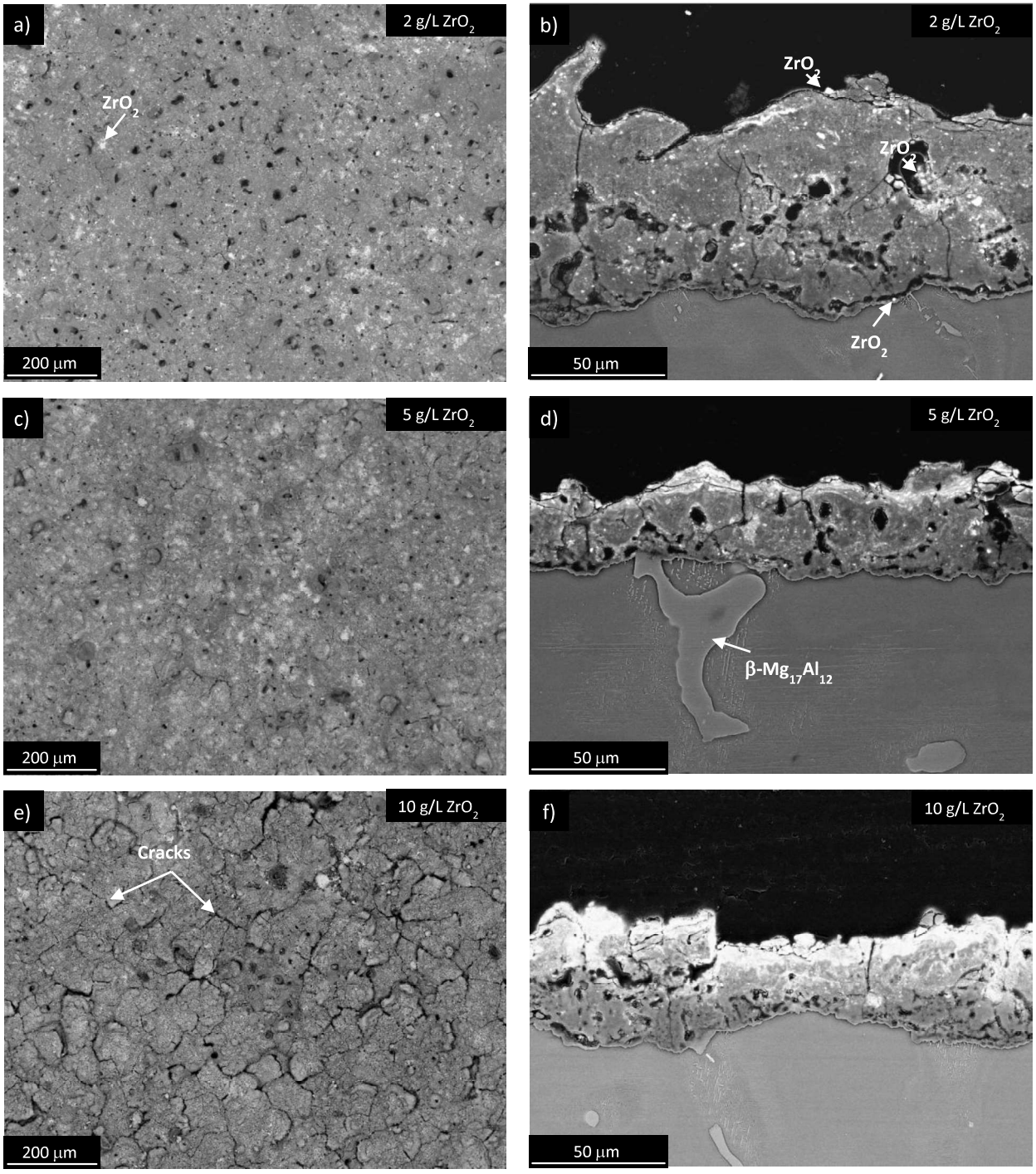
a)
2 g/L ZrO2
ZrO2
200 μm
b)
2 g/L ZrO2
ZrO2
ZrO2
ZrO2
50 μm
c)
5 g/L ZrO2
200 μm
d)
5 g/L ZrO2
β-Mg17Al12
50 μm
e)
10 g/L ZrO2
Cracks
200 μm
f)
10 g/L ZrO2
50 μm

Figure 3.

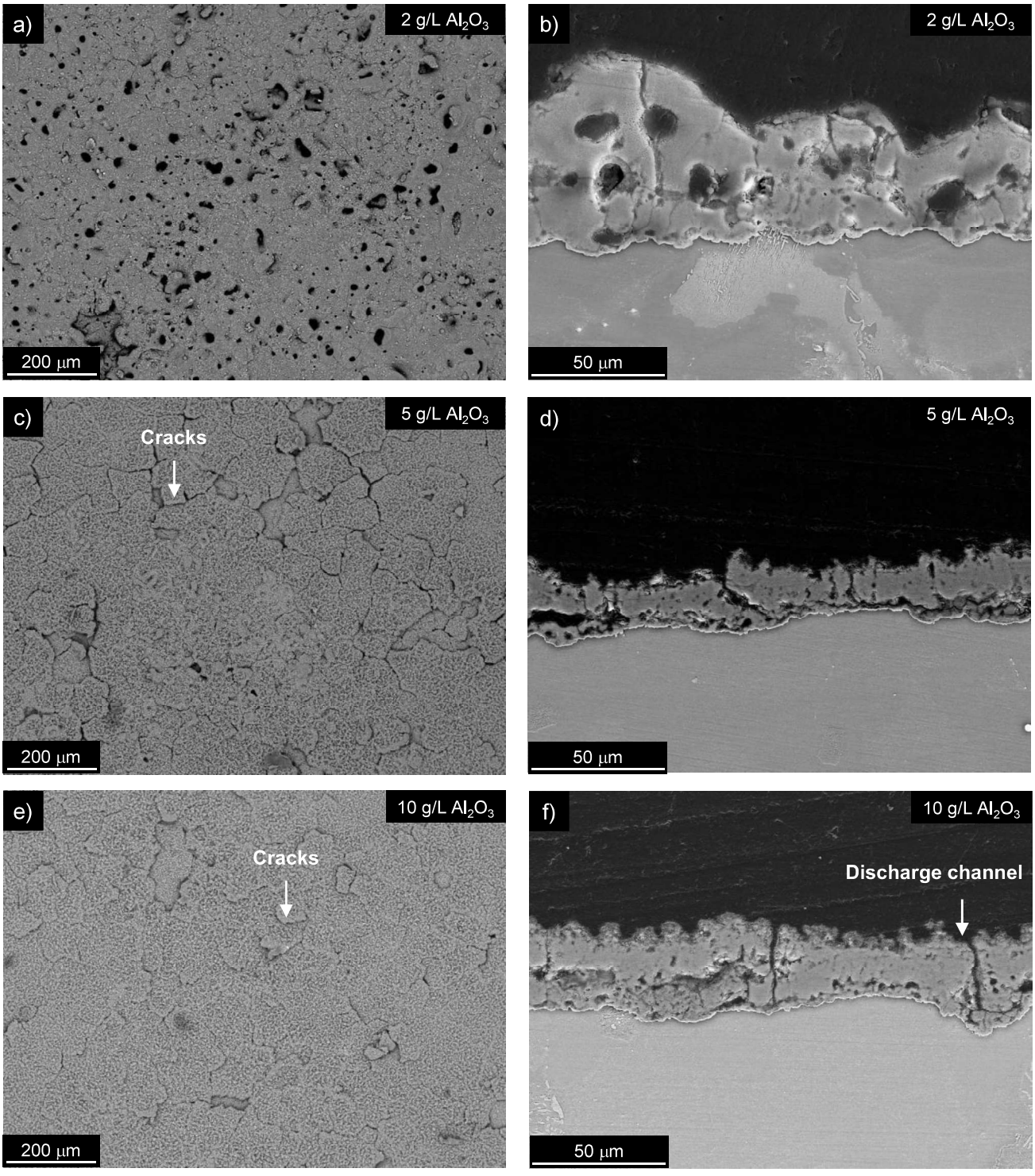
a)
2 g/L Al_2O_3
200 μm
b)
2 g/L Al_2O_3
50 μm
c)
5 g/L Al_2O_3
Cracks
200 μm
d)
5 g/L Al_2O_3
50 μm
e)
10 g/L Al_2O_3
Cracks
200 μm
f)
10 g/L Al_2O_3
Discharge channel
50 μm

Figure 4.

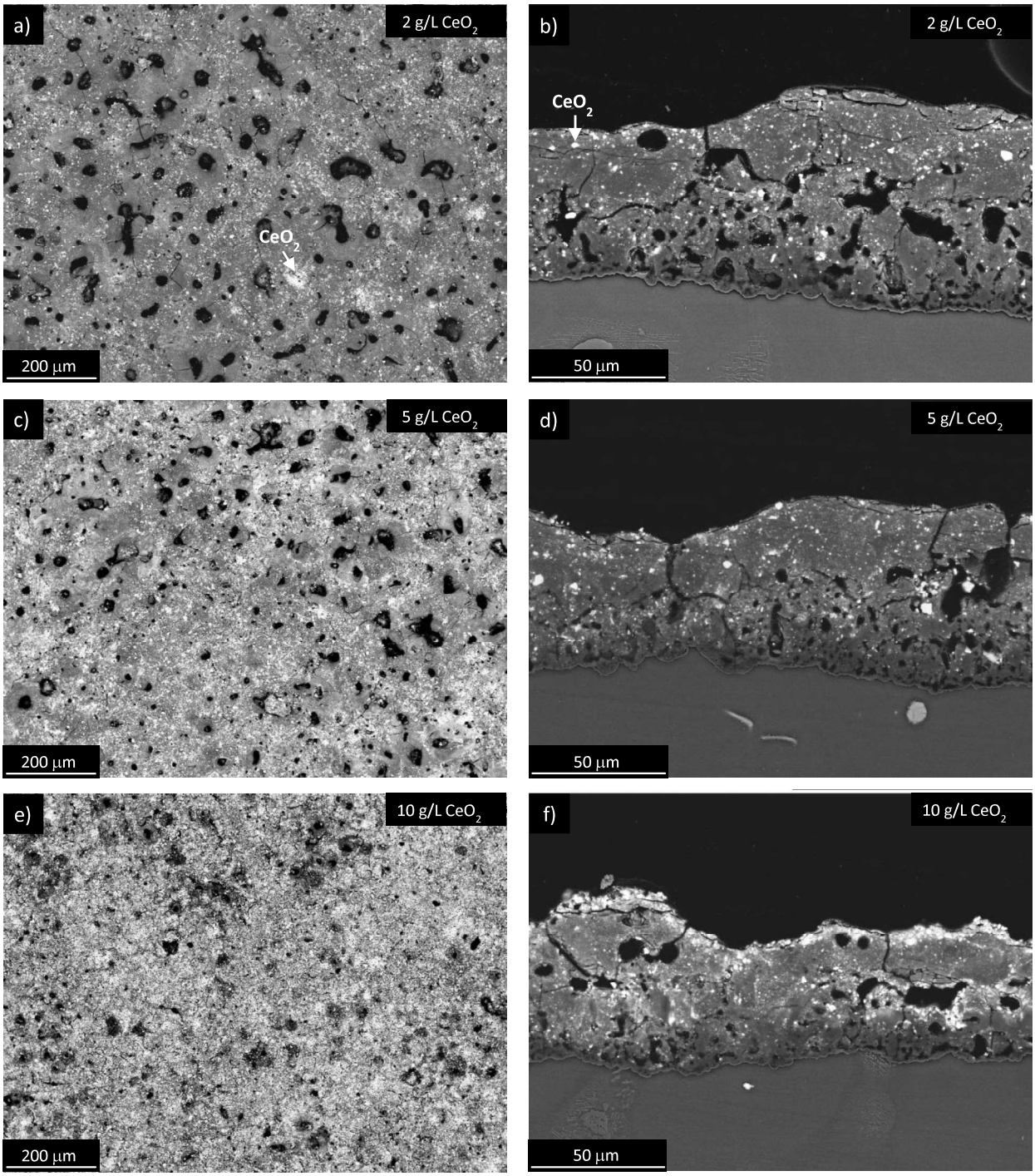
a)
2 g/L CeO2
CeO2
200 μm
b)
2 g/L CeO2
CeO2
50 μm
c)
5 g/L CeO2
200 μm
d)
5 g/L CeO2
50 μm
e)
10 g/L CeO2
200 μm
f)
10 g/L CeO2
50 μm

Figure 5.

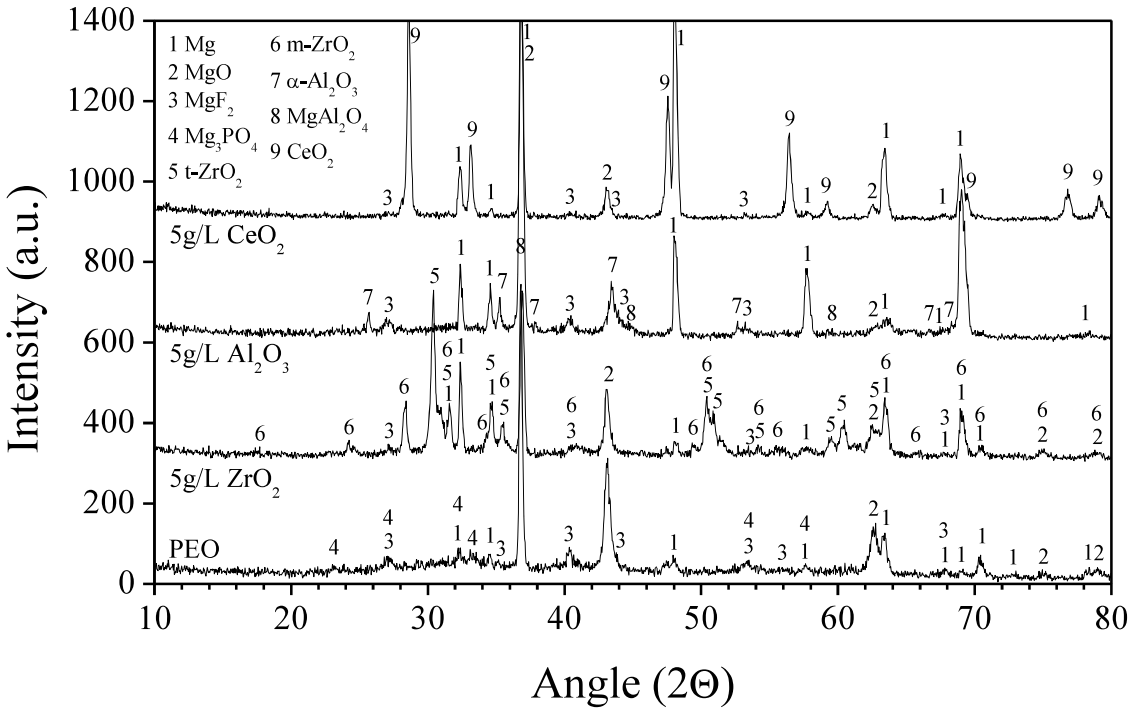
1 Mg
2 MgO
3 MgF2
4 Mg3PO4
5 t-ZrO2
6 m-ZrO2
7 α-Al2O3
8 MgAl2O4
9 CeO2
5g/L CeO2
5g/L Al2O3
5g/L ZrO2
PEO
Intensity (a.u.)
Angle (2Θ)

Figure 6.

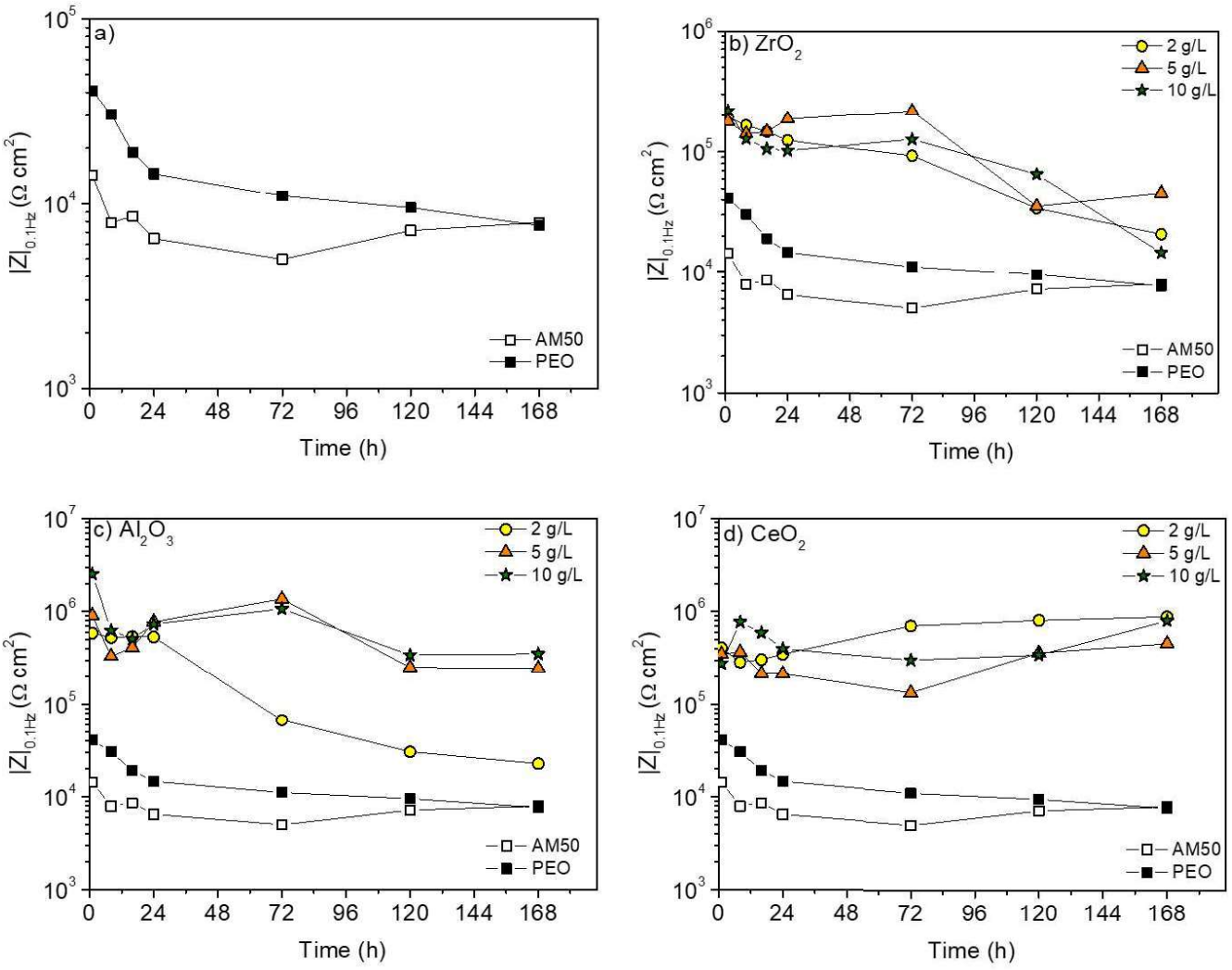

Figure 7.

Tables

Table1. EDS analysis (at.%) of the coatings formed on magnesium alloy AM50 with and without incorporated ZrO_2, Al_2O_3 and CeO_2 particles.

Coating	Particles (g/L)	Location	Elements (at.%)							
			Mg	Al	O	F	Na	P	K	Zr or Ce
PEO	0	Surface	22.63	0.48	36.21	24.84	22.63	5.26	0.23	
		Inner	25.00	1.14	29.03	28.97	7.88	6.55	0.31	
		Barrier	46.56	1.85	15.48	33.90	-	1.45	-	
ZrO_2	2	Surface	17.61	0.69	39.36	25.11	8.85	4.32	0.22	3.36
		Inner	30.25	1.30	20.38	39.64	5.94	1.18	0.08	1.24
	5	Surface	14.25	0.28	47.56	20.38	8.44	-	0.22	8.81
		Inner	33.96	1.92	29.43	23.83	1.77	5.77	-	1.33
	10	Surface	24.85	0.32	38.16	18.79	7.43	-	0.21	9.84
		Inner	33.89	5.60	30.48	22.70	2.03	3.85	0.17	1.27
		Barrier	48.14	4.54	22.84	20.61	0.18	2.33	-	0.15
Al_2O_3	2	Surface	15.96	7.96	40.49	21.54	8.72	4.14	0.23	
		Inner	27.17	4.20	26.38	30.84	4.16	4.96	0.20	
	5	Surface	11.94	15.44	51.64	11.97	5.20	2.89	0.21	
		Inner	28.44	8.24	28.03	27.19	1.35	4.16	-	
	10	Surface	8.72	20.74	57.44	7.19	3.35	2.09	0.12	
		Inner	31.16	5.01	22.96	33.58	-	4.73	-	
		Barrier	43.55	3.46	20.94	29.60	-	2.44	-	
CeO_2	2	Surface	20.37	0.73	34.25	27.00	10.09	4.64	0.24	2.03
		Inner	31.80	2.23	22.32	34.40	3.18	5.40	0.10	0.57
	5	Surface	21.88	0.53	38.61	20.46	8.37	4.50	0.21	4.33
		Inner	30.38	1.59	27.33	31.37	2.19	4.78	-	0.62
	10	Surface	17.56	-	45.22	14.42	8.28	3.98	0.27	9.06
		Inner	30.13	0.91	27.41	31.13	2.55	4.82	-	1.28
		Barrier	52.73	0.97	15.30	31.00	-	-	-	-

Table 2. The main characteristics of the PEO coatings: thickness, roughness and porosity.

Coating	Particles (g/L)	Thickness (µm)	Ra (µm)	Rz (µm)	% area with pores
PEO	0	112 ± 12	6.7 ± 0.2	38 ± 1	7
ZrO_2	2	81 ± 5	5.9 ± 0.8	36 ± 5	3
	5	57 ± 4	5.1 ± 0.3	31 ± 2	1.5
	10	55 ± 4	5.3 ± 0.5	31 ± 4	<1.5
Al_2O_3	2	62 ± 5	5.2 ± 0.8	30 ± 3	5
	5	31 ± 3	3.4 ± 0.3	22 ± 2	1.5
	10	27 ± 3	3.3 ± 0.1	21 ± 1	<1.5
CeO_2	2	90 ± 7	6.6 ± 0.9	37 ± 5	7
	5	73 ± 5	5.2 ± 0.3	30 ± 1	7
	10	54 ± 3	4.3 ± 0.1	28 ± 2	3

Figure
Click here to download Figure: Figures.docx

Figures

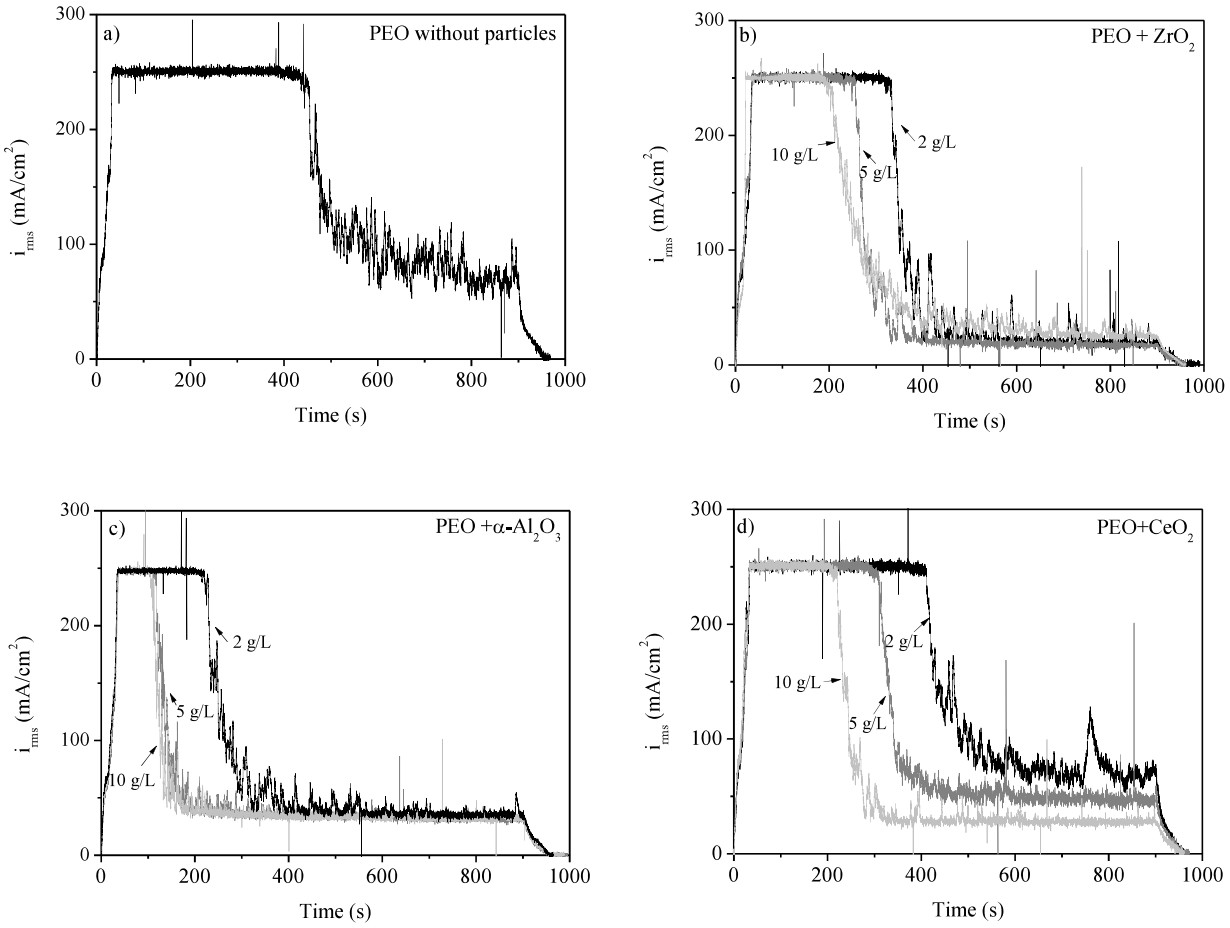

Figure 1.

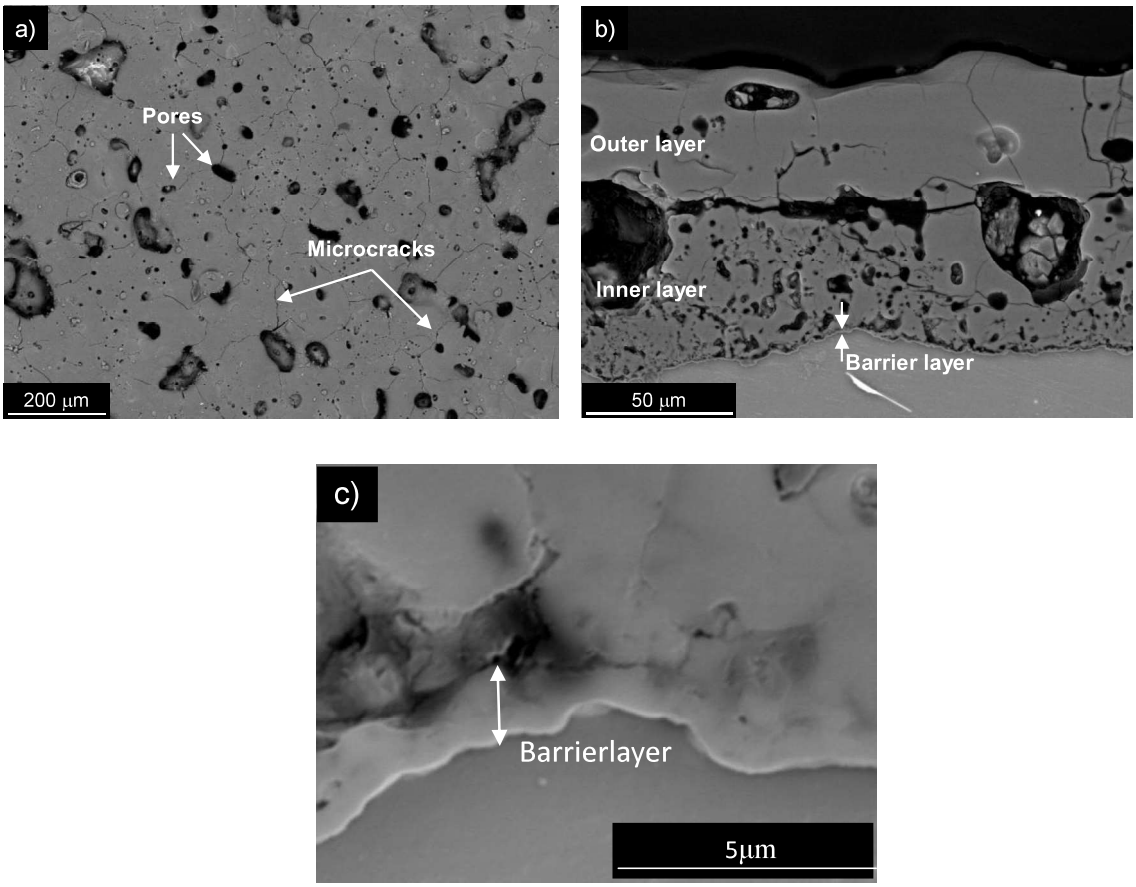
a)
Pores
Microcracks
200 µm
b)
Outer layer
Inner layer
Barrier layer
50 µm
c)
Barrierlayer
5µm

Figure 2.

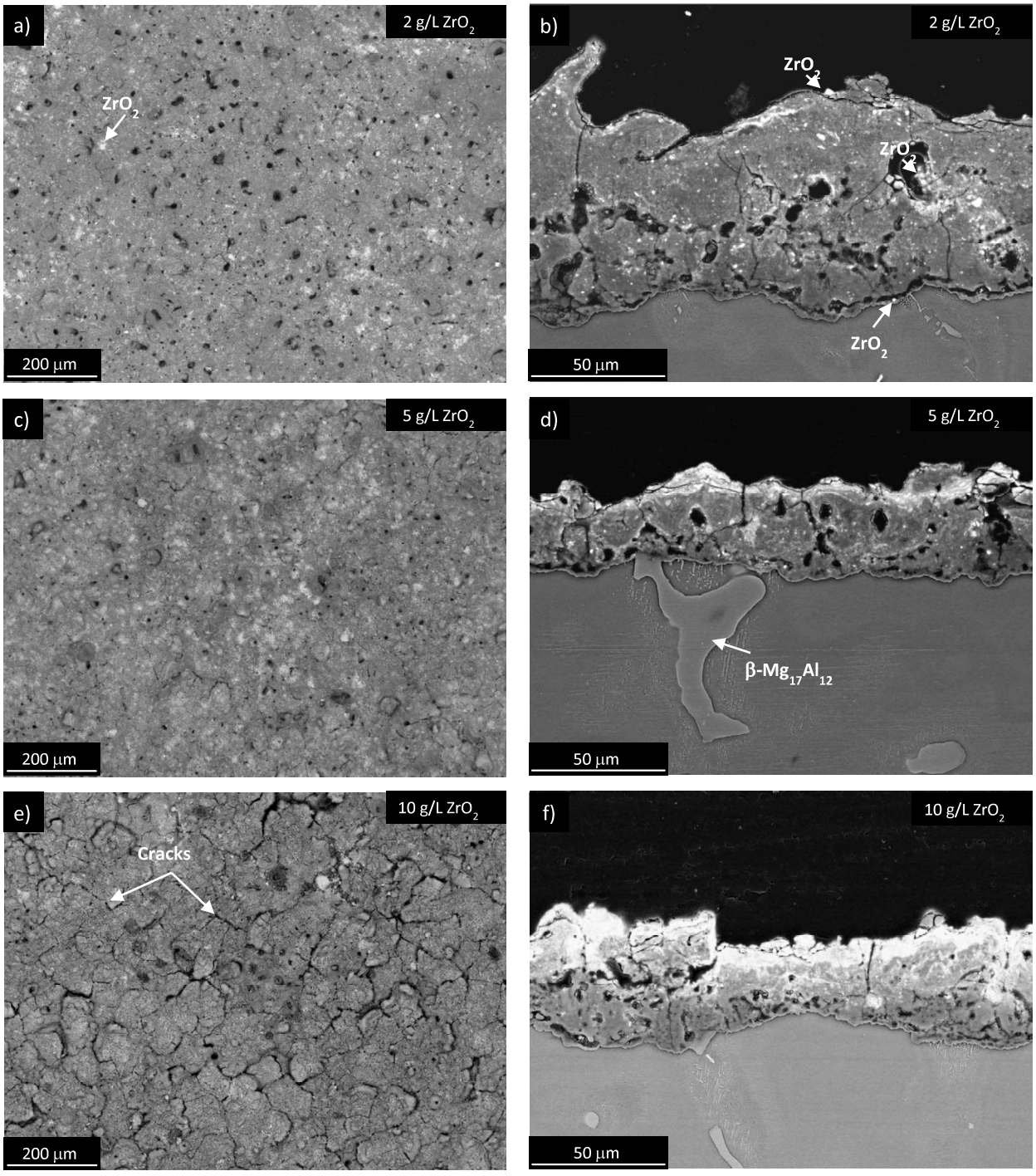
a)
2 g/L ZrO2
ZrO2
200 μm
b)
2 g/L ZrO2
ZrO2
ZrO2
ZrO2
50 μm
c)
5 g/L ZrO2
200 μm
d)
5 g/L ZrO2
β-Mg17Al12
50 μm
e)
10 g/L ZrO2
Cracks
200 μm
f)
10 g/L ZrO2
50 μm

Figure 3.

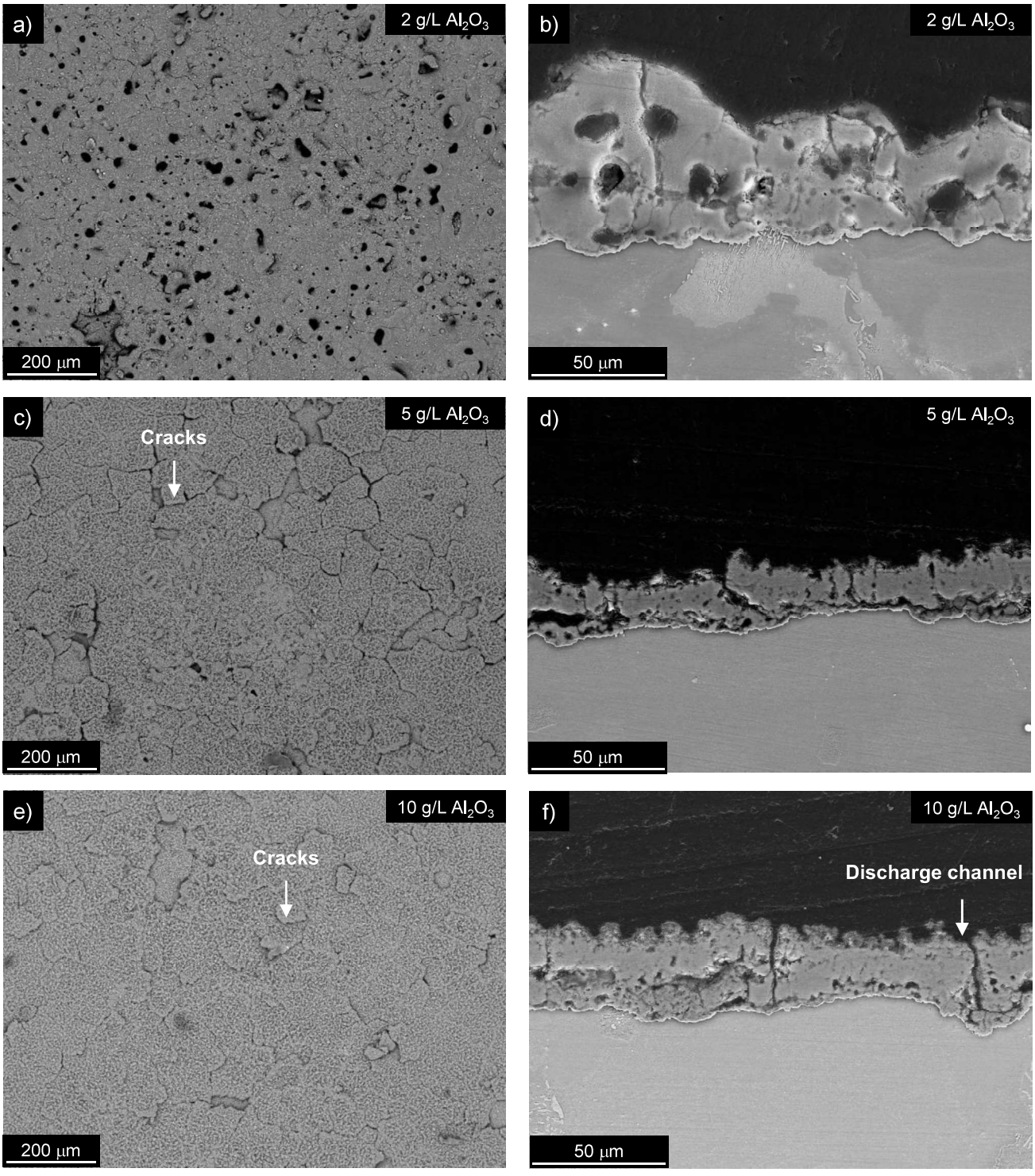
a)
2 g/L Al_2O_3
200 μm
b)
2 g/L Al_2O_3
50 μm
c)
5 g/L Al_2O_3
Cracks
200 μm
d)
5 g/L Al_2O_3
50 μm
e)
10 g/L Al_2O_3
Cracks
200 μm
f)
10 g/L Al_2O_3
Discharge channel
50 μm

Figure 4.

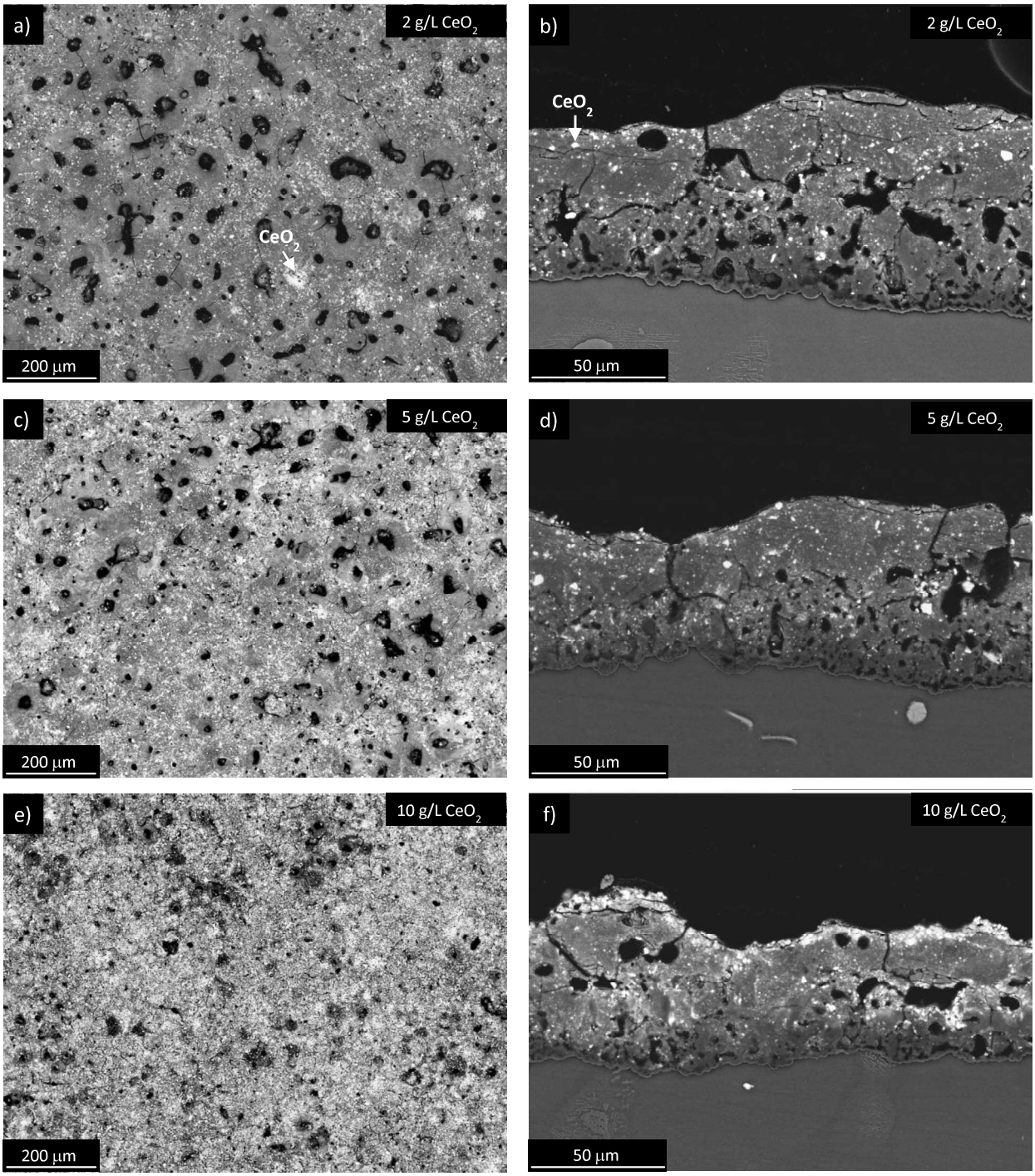
a)
2 g/L CeO2
CeO2
200 μm
b)
2 g/L CeO2
CeO2
50 μm
c)
5 g/L CeO2
200 μm
d)
5 g/L CeO2
50 μm
e)
10 g/L CeO2
200 μm
f)
10 g/L CeO2
50 μm

Figure 5.

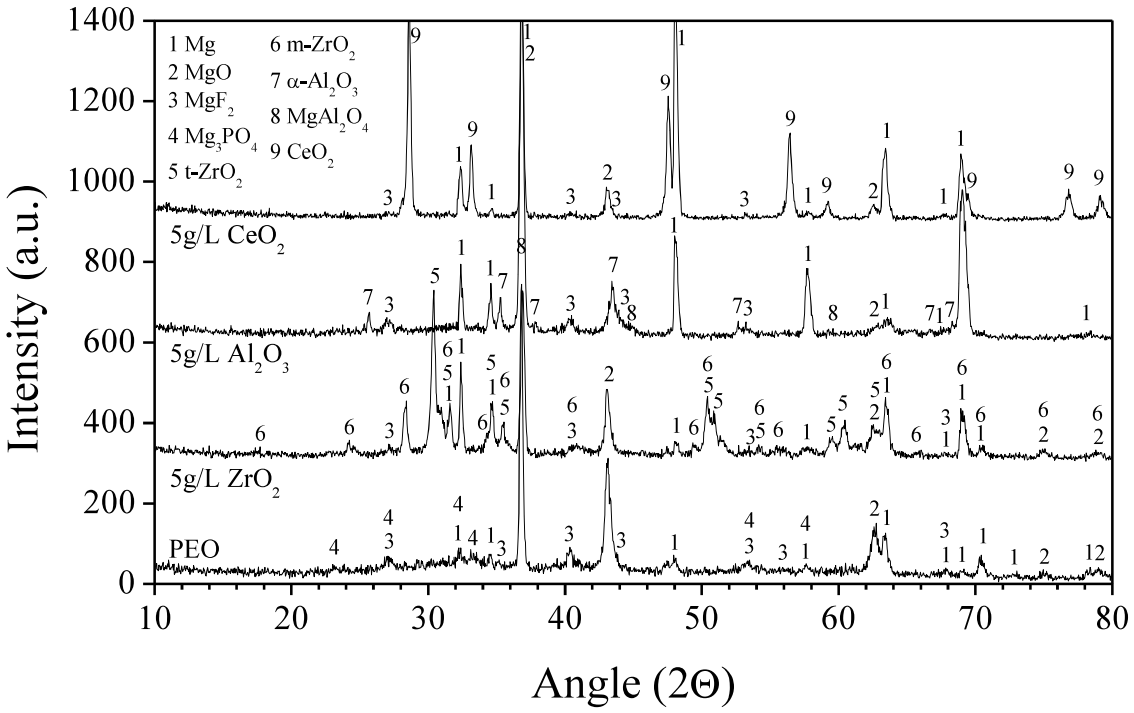
1 Mg
2 MgO
3 MgF2
4 Mg3PO4
5 t-ZrO2
6 m-ZrO2
7 α-Al2O3
8 MgAl2O4
9 CeO2
5g/L CeO2
5g/L Al2O3
5g/L ZrO2
PEO
Intensity (a.u.)
Angle (2Θ)

Figure 6.

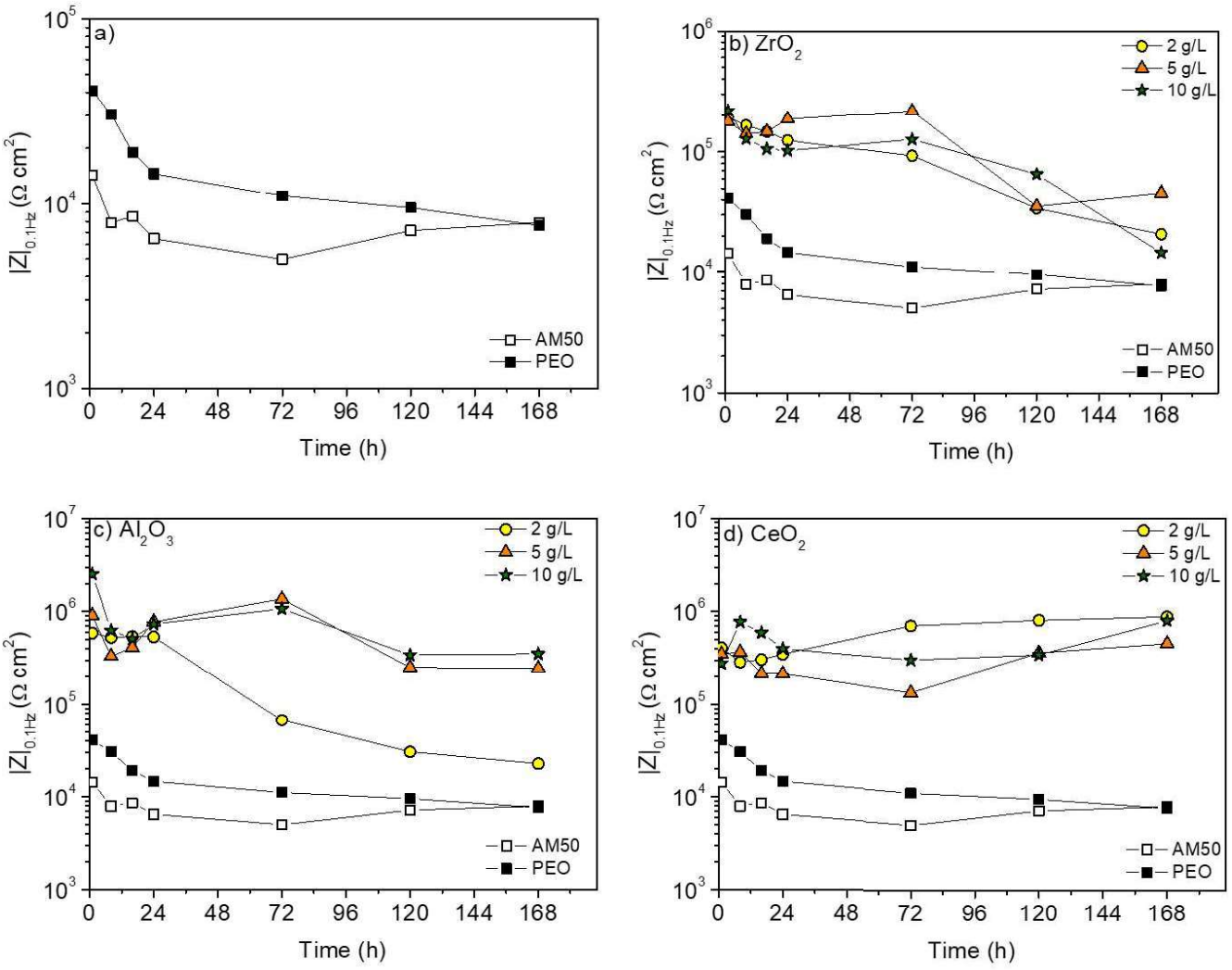

Figure 7.

*Suggested Reviewers

Suggested Reviewers

First Name	Last Name	Institution	E-mail Address
xiaopeng	**Lu**	Northeastern University	xiaopeng.Lu@hzg.de
luca	**Pezzato**	University of Padua	luca.pezzato@studenti.unipd.it
Xun	**Ma**	Helmholtz Zentrum Geestacht	xunm2013@gmail.com

All the reviewers have experience on developing Plasma electrolytic Oxidation coatings (PEO), characterization techniques and corrosion performance evaluation.

Graphical Abstract

Click here to download high resolution image